Mechanistic insights for the photoredox organocatalytic fluorination of aliphatic carbons by anthraquinone using time-resolved and DFT studies

J. W. Kee,[a] H. Shao,[a] C. W. Kee,[a,d] Y. Lu,*[a] H. S. Soo*[a,b,c] and C. H. Tan*[a]

Chemoselective photoredox fluorination is an appealing approach to access fluorinated fine chemicals such as active pharmaceutical ingredients, but most of the known procedures currently lack time-resolved mechanistic insights. We use nanosecond transient absorption spectroscopy and density functional theory (DFT) calculations to elucidate the elementary steps after irradiation in a photocatalytic fluorination procedure that we reported previously. Time-resolved optical spectroscopy suggests that direct reaction only occurs between the photoexcited anthraquinone (AQN) and Selectfluor®. We have observed spectroscopic evidence of a novel transient AQN-Selectfluor® species for the first time. Further studies by DFT calculations suggest that the AQN-Selectfluor® triplet exciplex formed by photoirradiation is responsible for initiating and sustaining the fluorination reaction.

Introduction

The fluorination of organic compounds has gained increasing significance in organic and medicinal chemistry because fluorinated compounds have become ubiquitous in drugs,[1-3] therapeutic imaging,[4, 5] materials science,[6] and agrochemicals.[7] In recent years, a number of protocols have been developed for the chemoselective synthesis of fluorinated fine chemicals and drugs.[8-15] For instance, Selectfluor® has been employed as the fluorine source for the radical fluorination of sp^3 C-H bonds[12, 16-21] and alkyl radicals generated from decarboxylation reactions.[22-27] Some groups, including our team, have demonstrated the photochemical radical fluorination of sp^3 C-H bonds (Scheme 1a).[13, 22-24, 28-34] Notably, our system is conducted at mild ambient temperatures, has a selective preference towards electron rich secondary C-H bonds,[29] and is consistent with the polar selectivity of cationic *N*-radicals reported previously.[15, 35-38] A detailed mechanistic study by

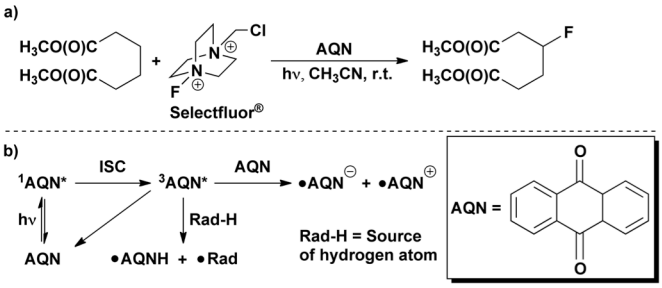

Scheme 1 (a) Photoredox fluorination protocol previously reported by our team. (b) Chemical processes after irradiation of AQN.

Lectka and co-workers supports our hypothesis that cationic *N*-radicals generated from Selectfluor® function as the hydrogen (H) abstractor.[15] In addition, our previously reported selectivity studies and density functional theory (DFT) calculations also suggested that the AQN photosensitizer initiated the selective photoredox chemistry via a reaction between the excited-state AQN[39] and Selectfluor® in a polar radical reaction under mild conditions.[15, 29, 36-38] A deeper understanding of these mechanistic differences is crucial in the further elaboration of our fluorination procedure to either asymmetric Selectfluor® derivatives[40] or enantiopure AQN photosensitizers.

There have been a considerable number of synthetic studies on the photochemical radical fluorination of sp^3 C-H bonds.[13, 22-24, 28-34, 41] However, few reports probe the mechanistic details of the radical fluorination process,[15] and none of them use time-resolved techniques to the best of our knowledge. Our team has been employing photochemistry for energy[42-45]

[a] Division of Chemistry and Biological Chemistry, School of Physical and Mathematical Sciences, 21 Nanyang Link, Nanyang Technological University, Singapore 637371.
E-mail: yplu@ntu.edu.sg, hansen@ntu.edu.sg, choonhong@ntu.edu.sg
[b] Singapore-Berkeley Research Initiative for Sustainable Energy (SinBeRISE), 1 Create Way, Singapore 138602.
[c] Solar Fuels Laboratory, Nanyang Technological University, 50 Nanyang Avenue, Singapore 639798.
[d] University of Oxford, Chemistry Research Laboratory, 12 Mansfield Road, Oxford OX1 3TA, UK.

†Electronic Supplementary Information (ESI) available: Detailed transient absorption spectroscopic measurements, Stern-Volmer quenching experiments, and DFT calculations. See DOI: 10.1039/x0xx00000x

and environmental applications,[43, 46] with a focus on building up our spectroscopic toolkit to monitor photoredox reactions.

Herein, we use transient absorption spectroscopic studies to demonstrate that AQN exclusively reacts with Selectfluor® to form an AQN-Selectfluor® exciplex (with similar spectroscopic signatures for several other fluorinating agents), whereas no direct reaction is observed between AQN and dimethyl adipate as a representative substrate. *The fact that the substrate does not react with the photoexcited AQN rules out H atom abstraction by triplet AQN during the initiation.* In addition, DFT[47] studies within this manuscript support the identity of our experimentally observed spectral signature of the AQN-Selectfluor® exciplex, and offer insights to the mechanistic pathway for this radical fluorination reaction. Notably, the exciplex possesses a transient interaction between the fluorine atom of Selectfluor® and the π-electron cloud of AQN, reminiscent of the C-F•••aryl interactions observed by Holl *et al.* recently.[48]

Results and discussions

Time-resolved optical spectroscopy on AQN

To begin, we sought to monitor the photochemical behavior of only AQN under reaction conditions that closely matched those of our previously reported photocatalytic processes.[29] We had shown that AQN solutions (~165 μM in O_2-free, anhydrous acetonitrile) could be irradiated with an 11 W broadband white light fluorescent lamp in the presence of Selectfluor® to fluorinate secondary sp^3 C-H bonds (Scheme 1a).[29] However, since AQN is colorless, we believe that the UV components of the light source are predominantly responsible for all the photochemistry. Thus, we employed 355 nm UV pulses in all our spectroscopic experiments with anhydrous, O_2-free acetonitrile as the solvent. For the transient absorption and emission spectroscopic (TAS and TES respectively) measurements, the samples were probed by a broadband xenon lamp beam before and after 4 – 6 ns pulses and the intensity of the transmitted light was detected. In all the transient absorption spectra in this manuscript, the detected signals are presented as the logarithm of the ratio (ΔOD) of the transmitted light intensity from the probe beam *after* laser excitation to the transmitted intensity *before* laser excitation. The ΔOD thus represents increased absorption (positive ΔOD) or reduced absorption/emission (negative ΔOD) of the transient photoexcited state relative to the ground state.

We measured the transient absorption spectrum of AQN between 365 and 805 nm. Under our experimental conditions with 165 μM AQN in acetonitrile, the transient absorption spectrum (red line, Fig. 1a) after irradiation with 355 nm nanosecond pulses differs from previously reported spectra of triplet ^{3}AQN*, which should exhibit bands with λ_{max} at 380 and 660 nm (black arrow, Fig. 1a).[49, 50] Instead, our transient absorption spectrum appears to correspond to a superposition of the AQN radical anion (•AQN$^-$) and the AQN semiquinone radical (•AQNH).[49, 51] The transient absorption spectrum of •AQN$^-$ has been shown to include a distinctive feature at 545 nm[51] (red square, Fig. 1a), which has a lifetime of 21.2 ± 0.2 μs under our experimental conditions (Fig. 1b). On the other hand, the transient absorption spectrum of •AQNH displays a broad absorption band centred at 745 nm (blue triangle, Fig. 1a), which can be fit to a longer-lived decay of 123 ± 1 μs. With our reaction conditions, the ^{3}AQN* can react with H atom sources in the solvent to form •AQNH.[52] Also, at high AQN concentrations, ^{3}AQN* has been observed to react with ground-state AQN to form the radical cation (•AQN$^+$) and •AQN$^-$.[53]

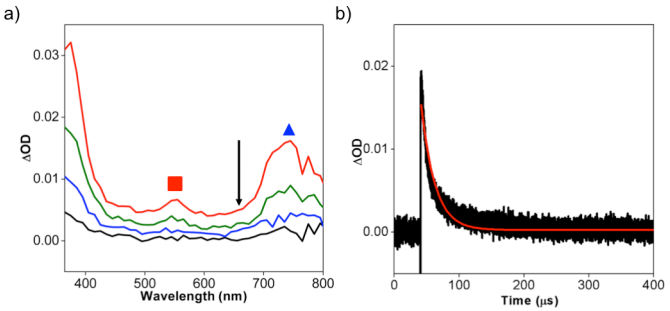

Figure. 1 (a) Transient absorption spectra of AQN at different concentrations (red: 165 μM, green: 83 μM, blue: 41 μM, black: 21 μM) obtained 2 μs after pulsed 355 nm irradiation. The black arrow indicates the absence of the reported peak at 660 nm expected for ^{3}AQN*.[49,50] (b) Transient absorption signal (black) of 165 μM AQN at 545 nm upon 355 nm pulsed irradiation of AQN. The red line is the mono-exponential fit for the decay, which matches the lifetime of •AQN$^-$.

Despite varying the concentration of AQN between 21 μM and 165 μM, *we did not observe the formation of ^{3}AQN** (missing peak at 660 nm, black arrow, Fig. 1a). We attributed this to differences in the pulse energies used previously (80-100 mJ/pulse),[49] thermal repopulation of the ^{1}AQN at room temperature,[54-56] and the high quantum yields of •AQNH formation at low light intensities.[52] This is especially apparent when the *relative* contribution of the longer-lived •AQNH species to the 375 nm signal increased upon lowering the pulse energies from 15 mJ/pulse to 2 mJ/pulse. Since the scope of this study is to investigate the mechanism as similar as possible to our previously reported photoredox reaction conditions, we did not probe the sample at higher irradiation intensities, lower temperatures, or with purified reagents and solvents, to access the triplet state.

We have further analyzed the decay lifetimes at 375, 455, and 745 nm. The •AQN$^-$ radical also absorbs at 375 nm, •AQNH has absorption signatures at both 375 and 745 nm, while the last is the absorption maximum of a new exciplex that we report here (*vide infra*). For instance, the temporal profile at 375 nm can be fit to a bi-exponential decay with a faster component (16.0 ± 0.2 μs) that can be attributed to the recovery of AQN from •AQN$^-$ (Table 1). A slower component (128 ± 1 μs) arises due to recovery of AQN from •AQNH (Table 1). Overall, the time-resolved optical spectroscopy suggests that the photochemical behavior of AQN at high concentrations and low irradiation intensities is more complicated than previously observed,[49] but AQN nonetheless

Table 1. Bi-exponential fits of the transient absorption decay signals at 375 nm, 455 nm, and 745 nm, after 355 nm irradiation of 165 µM AQN solutions in acetonitrile.

Wavelength	Decay lifetimes[a] (µs)	
	AQN	AQN + Selectfluor®
375 nm	**16.0 ± 0.2 (60%)**	**2.04 ± 0.02 (85%)[b]**
	128 ± 1 (40%)	108 ± 1 (15%)
455 nm	1.69 ± 0.02 (74%) [b]	**3.72 ± 0.04 (86%) [b]**
	120 ± 1 (26%)	65.9 ± 0.7 (14%)
745nm	10.5 ± 0.1 (62%)	2.39 ± 0.03 (83%)[b]
	123 ± 1 (38%)	123 ± 1 (17%)

[a] Relative contributions of the decay components are presented in parentheses. [b] Lifetimes shorter than 10 µs were fitted from transient absorption data within the first 15 µs.

reversibly reverts to its original ground state after each UV pulse for short illumination durations.

Quenching experiments with fluorinating agents

After acquiring an understanding of the photochemical features of AQN itself, we conducted TES experiments on AQN in the presence of fluorinating agents to probe the effect of potential quenching agents on the lifetime of the photoexcited AQN. Intriguingly, time-resolved measurements on solutions of AQN with 3.8 to 760 equivalents of Selectfluor® (0.63 to 126 mM) displayed different transient *emission* spectra from that obtained for AQN itself (Fig. 2). The emission spectrum of ^{3}AQN* was not observed, indicating that this *new species formed within the pulse-width of our excitation source.* We used 380 equivalents of Selectfluor® (63 mM) in majority of the experiments to match the same number of equivalents during the photoredox reactions if performed on the same scale. Notably, the transient absorption spectrum at 2 µs after 355 nm laser excitation exhibited a different profile (blue line, Fig. 3a) from the •AQN$^-$ and •AQNH species that we observed in the absence of Selectfluor® (red line, Fig. 3a). A new diagnostic shoulder

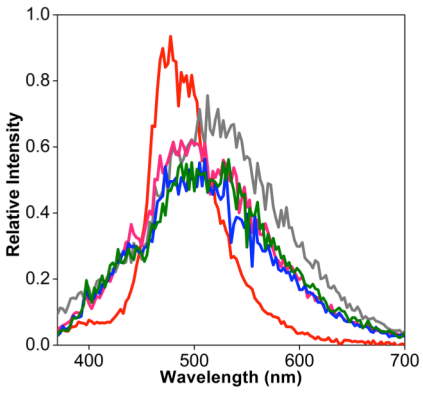

Figure. 2 Transient *emission* spectra of 165 µM AQN with different concentrations of Selectfluor® (green: 126 mM; blue: 63 mM; pink: 6.3 mM; gray: 0.63 mM) obtained 2 ns after pulsed 355 nm irradiation. The transient *emission* spectrum of 165 µM AQN only (red) is included for comparison.

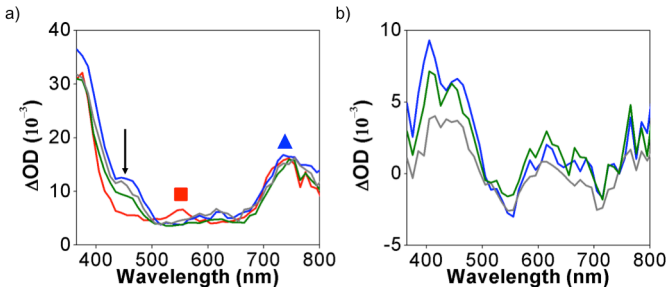

Figure. 3 (a) Transient absorption spectra of 165 µM AQN, in the presence of different fluorinating agents (red: none added, blue: 63 mM Selectfluor®, green: 63 mM Selectfluor® II, grey: 63 mM 1-fluorotrimethylpyridinium tetrafluoroborate) obtained 2 µs after pulsed 355 nm irradiation. The black arrow indicates the transient absorption signal assigned to the AQN exciplex. The red line is identical to the spectrum in red shown in Fig. 1a, and is presented here again to aid the comparison with the remaining three spectra. (b) Difference spectra obtained by subtracting the transient spectra of AQN from the corresponding normalized transient spectra of AQN (same color scheme as part (a) with the respective fluorinating agents (63 mM), obtained 2 µs after pulsed 355 nm irradiation).

at λ_{max} = 455 nm is discernible (black arrow, Fig. 3a), which can be attributed to the absorption of a •AQN-Selectfluor® triplet diradical according to our DFT studies (*vide infra*). *Since this new transient species formed without the intermediacy of the ^{3}AQN* radical within the pulse-width of our laser, it had arisen at rates faster than diffusion control, alluding to the formation of an exciplex.* Furthermore, •AQN$^-$ is no longer observed, as indicated by the absence of the absorption band at 545 nm (red square, Fig. 3a).

Under the oxidizing conditions with Selectfluor® present, the contribution of •AQNH to the transient absorption signal has diminished dramatically. This is clearly illustrated by the decay profile at 375 nm, where the long-lived component accounts for only 15% of the decay signal (Fig. 4a), instead of 40% for the signal without Selectfluor® (Table 1). Likewise, in the isolated region at 745 nm, the long-lived component shows a diminished contribution of 17%, instead of 38% in the absence of Selectfluor®. The band at 455 nm is convoluted by the superposition of multiple transient species (Table 1), but is clearly distinct from the data without Selectfluor® (Fig. 3a).

Subsequently, we performed measurements to determine the concentration-dependence of Selectfluor® on the lifetimes and absorption spectra of the transient species (Fig. S1a, Electronic Supplementary Information, †ESI). Interestingly, the decay lifetimes of the photoexcited transient species do not change systematically at different concentrations of Selectfluor® between 0.63 and 126 mM (Table S1, †ESI). Even at short time-scales, the decay lifetimes and transient absorption spectra remain similar (Fig. S1, †ESI) and these observations allude to the formation of a singlet excited state intermediate that decays to a longer-lived triplet AQN-Selectfluor® exciplex within the pulse-width of the UV photoexcitation source (*vide infra*).[48]

Furthermore, irradiation of AQN with other fluorinating agents such as Selectfluor® II and 1-fluoro-2,4,6-trimethylpyridinium BF_4 (F-Py) led to transient absorption spectra similar to when

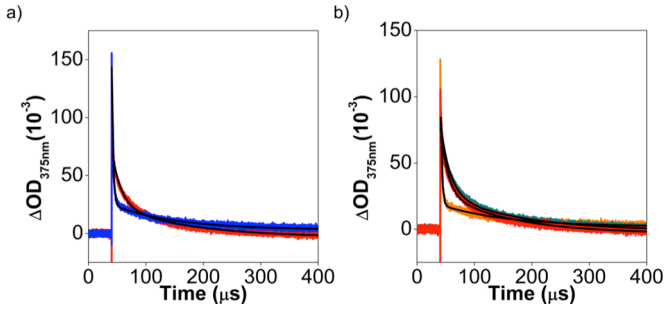

Figure. 4 (a) Transient absorption signal at 375 nm upon 355 nm pulsed irradiation of AQN only (red) and in the presence of Selectfluor® (blue). (b) Transient absorption signal at 375 nm upon 355 nm irradiation of AQN with 94 mM dimethyl adipate in the absence (cyan) and presence of Selectfluor® (orange). The black lines represent the bi-exponential fits for the respective decay signals.

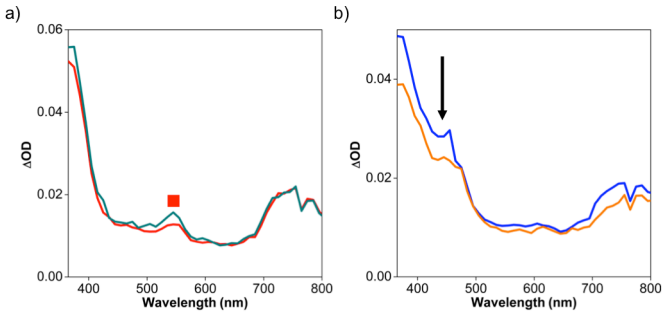

Figure. 5 (a) Transient absorption spectra of 165 µM AQN only (red), and in the presence of 94 mM dimethyl adipate (cyan), 2 µs after pulsed 355 nm irradiation, both of which show exhibit the signature of •AQN$^-$ (red square). (b) Transient absorption spectra of 165 µM AQN in the presence of 63 mM Selectfluor®, in the absence (blue), and in the presence of 94 mM dimethyl adipate (orange), 2 µs after pulsed 355 nm irradiation, with the distinctive signal from the AQN- Selectfluor® exciplex (black arrow).

Selectfluor® was used (grey and green lines, Fig. 3). The time decay at 455 nm with these fluorinating agents (Fig. S2, †ESI) are also similar to the lifetime when Selectfluor® was used.

The fact that disparate fluorinating agents react with AQN to produce similar transient spectral profiles (Fig. 3) and lifetimes (Tables S1 and S2, †ESI) suggest that the exciplex consists of AQN activated by an electrophilic source of F in close proximity. When comparing the transient absorption spectra, the ΔOD at 455 nm 2 µs after photoexcitation is higher for Selectfluor® than both F-Py and Selectfluor® II, indicating that Selectfluor® is most effective at producing this transient AQN exciplex (Fig. 3). However, the signal for Selectfluor® II is lower than that of F-Py, which is likely due to the lower solubility and hence reduced concentration of Selectfluor® II during the experiments. By comparing the reduction potentials of the fluorinating agents (Selectfluor®: –0.04 V; Selectfluor® II: –0.09 V; F-Py: –0.73 V vs standard calomel electrode),[57, 58] the trend in ΔOD appears to correlate with the thermodynamic driving force for fluorine transfer to AQN, after correction for differences in the solubility of the fluorinating agents. With these data in hand, the difference spectra between AQN *with* the fluorinating agents, and the spectrum of AQN *without* fluorinating agents can be produced (Fig. 3b). The difference spectra in the presence of fluorinating agents exhibit a diagnostic band of λ_{max} around 425 nm, which is supported by our DFT calculations below.

Quenching experiments with aliphatic substrate

Following these experiments, we explored whether dimethyl adipate itself could quench the photoexcited AQN in the absence of Selectfluor®. Dimethyl adipate was chosen as a substrate with sufficiently high solubility in acetonitrile, without any intrinsic photochemistry upon irradiation with 355 nm laser pulses. *On the contrary, the transient absorption spectrum of AQN with dimethyl adipate only remains largely unchanged compared to AQN itself*, showing the presence of •AQN$^-$ (red square, Fig. 5), with the excited state decay lifetime at 375 nm similar to the values in the absence of fluorinating agents (c.f. 375 nm data in Tables 1 and 2). *The fact that the substrate does not react with the photoexcited AQN rules out H atom abstraction by triplet AQN during the initiation*, another plausible initiation process that is clearly not operational based on our spectroscopic measurements. In three-component solutions with AQN, Selectfluor®, and dimethyl adipate, the initial photoexcited state characteristics (Fig. 5b) coincide with those containing only AQN and Selectfluor®. Evidently, the substrates, with dimethyl adipate as a representative member, do not directly react with the photoexcited AQN, since no dramatic changes to the time-resolved spectroscopic behavior are observed. Instead, the data concur with a reaction path where photoexcited AQN reacts with Selectfluor® to form an AQN-Selectfluor® exciplex (black arrow, Fig. 5b), which we have observed here for the first time experimentally. Since the cationic *N*-radicals and substrate radicals do not possess spectral signatures in the

Table 2. Bi-exponential fits of the TAS decay signals at 375 nm, 455 nm, and 745 nm after pulsed 355 nm irradiation of 165 µM AQN *and* 94 mM dimethyl adipate with and without 63 mM Selectfluor®.

Wavelength	Decay lifetimes[a] (µs)	
	94 mM dimethyl adipate	94 mM dimethyl adipate and 63 mM Selectfluor®
375 nm	**17.2 ± 0.2 (65%)**	1.97 ± 0.02 (86%)[b]
	141 ± 2 (35%)	117 ± 1 (14%)
455 nm	2.42 ± 0.03 (74%)[b]	**3.53 ± 0.04 (87%)[b]**
	120 ± 1 (26%)	216 ± 2 (13%)
745nm	22.9 ± 0.3 (63%)	2.76 ± 0.03 (88%)[b]
	208 ± 2 (37%)	170 ± 2 (12%)

[a] Relative contributions of the decay components are presented in parentheses. [b] Lifetimes shorter than 10 µs were fitted from transient absorption data within the first 15 µs.

wavelength range of our experiments, we are able to spectrally detect the AQN-Selectfluor® exciplex exclusively.

We can now attribute the remarkable selectivity for fluorination reactions in our previous report[29] to the controlled abstraction of secondary H atoms from sites furthest from electron-withdrawing groups due to the polar transition states.[15, 36-38] The cationic AQN-Selectfluor® exciplex kinetically prefers to abstract the more electron-rich sp^3 C-H bond to form a more stable radical during the reaction.[15, 36-38] No systematic concentration dependence on dimethyl adipate (Tables 2 and S3, †ESI) is detected at 375 nm during laser flash photolysis with AQN only because the photoexcited AQN does not react with the substrates directly.

We observed a decrease in both the intensity and lifetime of the transient signal of the AQN-Selectfluor® exciplex at 455 nm as the concentration of dimethyl adipate increases from 1.5 to 12 equivalents (Fig. S3, †ESI). A Stern-Volmer plot (Fig. S4, †ESI) was obtained from the decay lifetimes of transient signal at 455 nm arising from the AQN-Selectfluor® exciplex in the presence of varying amounts of dimethyl adipate, and yielded a quenching rate constant k_q of 1.5 ± 0.1 × 10^5 $M^{-1}s^{-1}$. In the absence of dimethyl adipate, the AQN-Selectfluor® exciplex likely decays back to AQN and Selectfluor®. When dimethyl adipate is present, the exciplex is expected to initiate a chain reaction with the substrate to give HF and alkyl radicals, the latter of which can then react with more Selectfluor® or the transient exciplex to give the fluorinated product. The quantum yield for the fluorination reaction was determined through the well-studied ferrioxalate actinometer (see †ESI).[43, 59] However, a quantum yield of 0.13 was obtained, suggesting either a closed catalytic loop or inefficient chain processes instead.[60] The reaction could also be complicated by the formation of the cationic *N*-(chloromethylated)-1,4-diazabicyclo[2.2.2]octane (*vide infra*) as a side product, which is known to form a 1:1 adduct with Selectfluor®.[61] Attempts to trap the cationic Selectfluor® *N*-radical and alkyl radical intermediates with TEMPO and nitrosobenzene were unsuccessful, since these reagents appear to interfere with the photochemistry between AQN and Selectfluor®.

The steady-state absorption spectra before and after laser flash photolysis (Fig. 6a) concur with the model that we have proposed below (Fig. 7 – 9). In the *absence* of Selectfluor®, the UV-vis spectra with or without substrates present display characteristic vibronic structure with a λ_{max} = 380 nm, which can be attributed to the formation of 9,10-dihydroxyanthracene (DHA, black arrow, Fig 6a) from the disproportionation of •AQNH. Under the reaction conditions, ^{3}AQN* form •AQNH and •AQN^-, which can eventually lead to DHA in a series of disproportionation and acid-base reactions.[39, 49] On the other hand, the UV-vis spectra after photolysis of AQN with the fluorinating agents results in gradual photobleaching of AQN's UV absorption signals, but the characteristic absorption bands of DHA were not observed (Fig. 6b). The oxidizing environments in the presence of the cationic fluorinating agents preclude the formation of the reduced DHA.

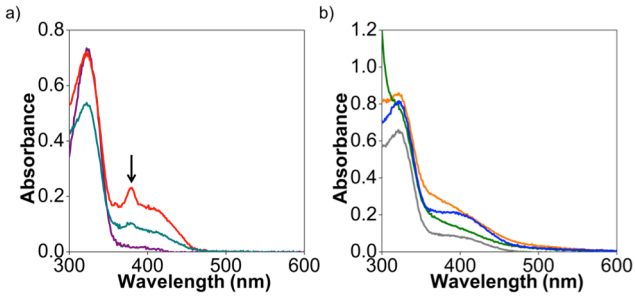

Figure. 6 (a) UV-vis spectra of AQN after transient absorption measurements without (red) and with dimethyl adipate (cyan). The black arrow indicates the appearance of 9,10-dihydroxyanthracene after transient absorption measurements. The UV-vis spectrum of AQN only before photolysis (purple) is included for comparison. (b) UV-vis spectra of AQN after transient absorption measurements in the presence of Selectfluor® (blue), Selectfluor® II (green), F-py (grey) or both Selectfluor® and dimethyl adipate (orange). All spectra were collected in acetonitrile solutions.

NMR spectroscopy and mass spectrometry

NMR spectroscopy and mass spectrometry were employed to probe the identity of the photobleached products. AQN is largely unchanged upon photolysis while Selectfluor® photodegrades in the presence of AQN to give the cationic *N*-(chloromethylated)-1,4-diazabicyclo[2.2.2]octane, which could be due to H abstraction by the cationic Selectfluor® *N*-radicals from impurities in acetonitrile. Acetonitrile itself is unlikely to be the source of H atoms since stronger C-H bonds from cyclohexane[62] (bond dissociation energy = 99 kcal mol^{-1}) have been known to be activated even if acetonitrile[63] (bond dissociation energy = 93 – 96 kcal mol^{-1}) is the solvent. Acetonitrile is known to be resistant to H atom abstraction due to its oxidative stability and is the solvent of choice for electrochemical experiments. A fluoride-containing product, with a ^{19}F NMR chemical shift at -183.8 ppm (with a negative value presented in the current sign convention), resembles that of HF in acetonitrile.[64] However, since we used borosilicate glass NMR tubes, HF will likely etch the glass and we postulate that this signal originated from a solvated F^-, a result of the AQN-Selectfluor® exciplex photodegradation in the absence of substrate.

DFT and TD-DFT calculations

Equipped with the spectroscopic detection of the new exciplex, we sought structural confirmation of its identity through TD-DFT calculations (see †ESI). The calculated absorption spectrum of the AQN-Selectfluor® exciplex exhibits an absorption band centered around 433 nm (Fig. 7b). The lowest energy visible bands (Table S25, †ESI) mostly include the excitation from the highest occupied molecular orbital (HOMO) to lowest unoccupied molecular orbital (LUMO) and HOMO-1 to LUMO, according to the orbital characters from the TD-DFT calculations. All these orbitals are delocalized over the entire exciplex with greater density on the π-orbitals of

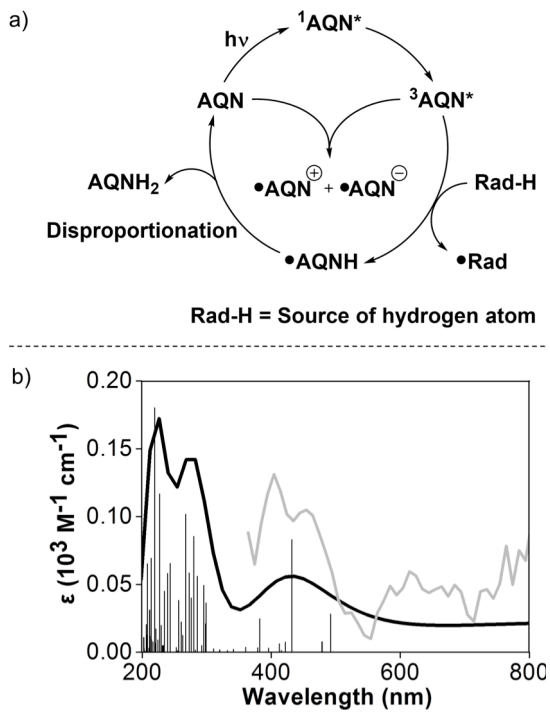

Figure. 7 (a) Proposed reaction pathways for AQN after 355 nm photoexcitation in acetonitrile in the absence substrate. (b) The TD-DFT calculated UV-vis absorption spectra. The black vertical lines represent the oscillator strengths from TD-DFT results and the observed transient absorption spectrum for the AQN-Selectfluor® exciplex from Fig 3b is in dark grey.

AQN. These calculated UV-vis bands of the exciplex are similar to the transient spectra that we observe (Fig. 3b and 7b). We screened several functionals to identify a good match between our observed spectroscopic data and the TD-DFT predicted spectra, since Singleton and coworkers have recently highlighted how the calculated reaction barriers for a number of organic reactions can be very sensitive to the functional applied.[65, 66] However, our preliminary calculations with other functionals suggested that they were not suitable for handling the open-shell systems in our study.

The reaction mechanism of AQN in the presence of Selectfluor® and pentane as a representative sp^3 hybridized substrate was further investigated with unrestricted spin DFT calculations by using the WB97XD functional and the 6-311G+(2d) basis set. All the calculations were performed with the Gaussian 09 software. We monitored the total spin of these compounds in the calculations and found that the differences between the calculated values and theoretical expectation values are very small (below 1%), so spin contamination is not a concern in these cases. Frequencies in the gas phase and solvent (acetonitrile), as well as thermodynamic data were calculated based on the ideal gas approximation.

As shown in Fig. 8a, AQN and Selectfluor® (**S_0**) can interact to form a van der Waal's complex **RC1**, which can be photoexcited to a short-lived **S_1** state after irradiation with an

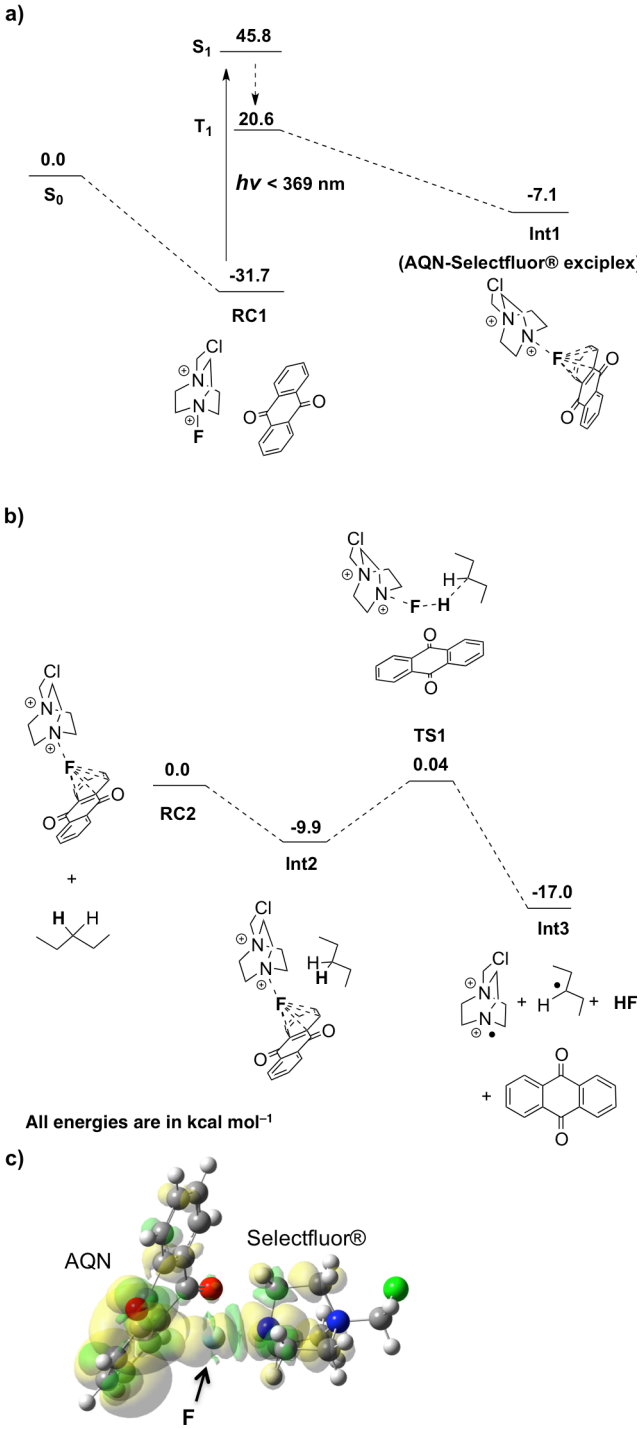

Figure. 8 Proposed reaction pathway from DFT calculations for the initiation of the radical fluorination process by (a) formation of the AQN-Selectfluor® exciplex in **Int1**, and (b) generation of the secondary pentane and Selectfluor® *N*-radicals from the exciplex. (c) Depiction of the spin density for the triplet AQN-Selectfluor® exciplex. Note the significant spin density on the fluorine atom of the elongated N-F bond bridging Selectfluor® and AQN. All energies are the electronic energies presented in kcal mol^{-1}.

electronic energy gap of about 77.5 kcal mol^{-1}. This energy gap

corresponds to a photon of ~369 nm, which concurs with the fact that common, 11 W household lamps and our 355 nm nanosecond pulses have the requisite energy to trigger this photoexcitation. Intersystem crossing will occur in an exothermic, non-radiative relaxation from the S_1 to the T_1 state, after which a spontaneous intramolecular reorganization process will occur to give the AQN-Selectfluor® exciplex (**Int1**). The structure of **Int1** concurs with the crystallographic fluorine-arene π-complex reported recently.[48] No transition state was detected by DFT calculations and this AQN-Selectfluor® exciplex exhibits a dramatically lengthened N-F bond distance of 2.0 Å (from 1.3 Å originally in Selectfluor®) and an average C-F bond distance of 2.9 Å. This suggests that the AQN-Selectfluor® exciplex possesses a highly activated transferable fluorine with the fluorine atom stabilized by one of the aromatic rings of AQN. The spin density is predominantly delocalized over AQN and F (61%), with smaller contributions from the rest of Selectfluor® (Fig. 8c). Since the optical absorption bands are largely dictated by the AQN-F interactions (Selectfluor® is aliphatic and colorless), the transient absorption spectra will be independent of the electrophilic fluorinating agent employed.

Subsequently, this reactive AQN-Selectfluor® exciplex can initiate the radical fluorination process by abstracting a hydrogen atom from the pentane model substrate (Fig. 8b). The weakest sp^3 hybridized secondary carbon would react to yield a secondary pentane radical, a Selectfluor® *N*-radical, HF, and AQN, with a thermally accessible activation barrier of only 9.9 kcal mol^{-1} (Fig. 8b).

The active Selectfluor® *N*-radical formed from the dissociation of **Int3** can then react with a secondary C-H bond in pentane to readily overcome a thermally accessible activation barrier of merely 2.0 kcal mol^{-1} in the exothermic reaction from **Int4** to **Int5** via **TS2** (Fig. 9a). Concurrently, the secondary pentane radical could also react in a facile fashion with Selectfluor® to surmount another thermally accessible activation barrier of only 7.6 kcal mol^{-1} between **Int7** and **Int8** via **TS3** in the highly exothermic fluorine atom transfer process (Fig. 9b). The radical intermediates in both processes can then propagate the chain reaction. Alternatively, a pentane radical can react with the AQN-Selectfluor® exciplex through a barrierless fluorine atom transfer process due to the extremely exothermic nature of this step (Fig. 9c). All the reaction pathways that we have considered are thermodynamically and kinetically feasible under ambient conditions based on our DFT calculations. However, since the quantum yield that we measured for this photoredox fluorination process is only 0.13, the chain propagation is likely to be inefficient, indicating that the direct, barrierless fluorination by the AQN-Selectfluor® exciplex is necessary for sustaining this radical fluorination process.

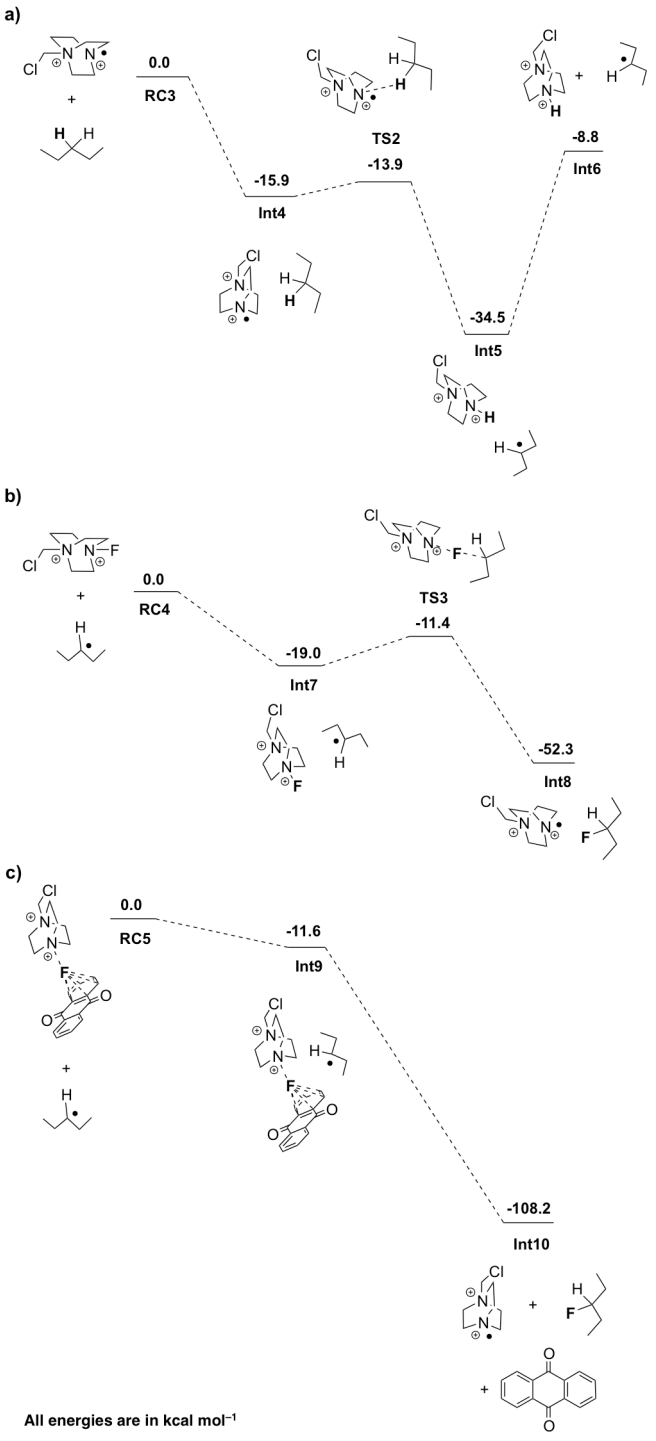

Figure. 9 Proposed reaction pathway from DFT calculations for the propagation of the radical fluorination process through (a) hydrogen atom abstraction by the Selectfluor® *N*-radical from pentane to give a secondary radical, (b) fluorine atom transfer from Selectfluor® to the pentane radical to yield 3-fluoropentane and the Selectfluor® *N*-radical, and (c) barrierless fluorine atom transfer from **Int1** to the pentane radical to yield 3-fluoropentane, AQN, and the Selectfluor® *N*-radical. All energies are the electronic energies presented in kcal mol^{-1}.

Experimental

General information

All chemicals were obtained from Sigma-Aldrich and used as received without further purification. Deuterated solvents were purchased from Cambridge Isotope Laboratories and

were used as received. Anhydrous acetonitrile, which was used in all optical spectroscopic measurements, was collected from an Inert PureSolv MD5 solvent purification system prior to being degassed on a Schlenk line using several freeze-pump-thaw cycles. All solutions were prepared in a glovebox and transferred into a modified Schlenk apparatus fused with a quartz fluorimeter cuvette (Starna, 10 mm pathlength) before transient absorption and emission measurements were performed. UV-visible spectroscopic measurements were performed using a Shimadzu UV-3600 UV-vis-NIR spectrophotometer and steady-state photoluminescence measurements were conducted using a Varian Cary Eclipse fluorescence spectrophotometer in acetonitrile. The ^{1}H and ^{19}F NMR spectra were recorded at room temperature on a Bruker AVANCE 400 MHz spectrometer. The ^{1}H NMR chemical shifts (δ reported in ppm) were referenced to the residual solvent signal(s) while the ^{19}F NMR chemical shifts were referenced internally to α,α,α-trifluorotoluene (-63.72 ppm vs $CFCl_3$ in the current sign convention with negative chemicals shifts). Solutions of anthraquinone (AQN) were prepared by diluting a 1.65 mM stock solution of AQN (10.3 mg, 0.0495 mmol in 30.0 ml of degassed acetonitrile).

Transient absorption measurements

The transient absorption and emission measurements were performed using an Edinburgh Instruments model LP920 transient absorption spectrometer equipped with a pulsed Xe probe lamp in conjunction with a Nd:YAG laser (Continuum model Surelite II-10) as the excitation source. The laser pulse width is 4-6 ns and the repetition rate is 10 Hz. During transient absorption measurements, the pulses are synchronized with the LP920 system at a frequency of 1 Hz. The pulse energy used was between 6-20 mJ/pulse.

The data were fit to single exponential or biexponential functions to obtain the time constants for the transient signals according to the following two equations respectively:

$$y = y_0 + A_1 e^{-(t-\tau_0)/\tau_1}$$
$$y = y_0 + A_1 e^{-(t-\tau_0)/\tau_1} + A_2 e^{-(t-\tau_0)/\tau_2}$$

The parameters y_0, τ_0, A_n and τ_n were determined by a least-squares fitting procedure in OriginPro. The term y_0 corresponds to the vertical intercept at long lifetimes and indicates whether the signal decays to a 'permanent' bleach (negative y_0) or absorption (positive y_0). The variable τ_0 is the delay time of the excitation pulse from the start of the probe measurement during each photoexcitation cycle. A_n is the change in optical density after irradiation for the nth exponential term and t_n is the corresponding time constant. The relative contribution of the nth term to the overall transient signal, c_n, was calculated using the following formula:

$$c_n = A_0/(A_1 + A_2)$$

Quantum yield measurements

Potassium ferrioxalate ($K_3[Fe(OX)_3]\bullet 3H_2O$, OX = oxalate) is a standard chemical actinometer for the determination of quantum yields for photochemical reactions under visible light in an aqueous medium.[67] Since the photoredox fluorination is performed in CH_3CN, it is necessary to use a chemical actinometer that functions in CH_3CN. Previously, our group has synthesized (n-$Bu_4N)_3[Fe(OX)_3]$ for this purpose and found that its quantum yield is 0.966 at 334 nm under AM1.5 irradiation.[43] Similarly, we have adopted this value and the same AM1.5 irradiation source to determine the quantum yield of the photoredox fluorination under AM1.5 irradiation.

The quantum yield of a photoreaction can be calculated using the equation:

$$\Phi_2 = (f_1 \bullet \Phi_1 \bullet r_2) / (f_2 \bullet r_1),$$

where Φ_1 = a known quantum yield of a reference photoreaction,
r_1 = rate of reference photoreaction,
f_1 = fraction of light absorbed by the photoactive species in the reference photoreaction,
r_2 = rate of the photoreaction investigated,
f_2 = fraction of light absorbed by the photoactive species in the photoreaction investigated,
Φ_2 = quantum yield of the photoreaction investigated.

A 0.60 mL solution of 118 μM AQN with 44 mM Selectfluor® and 66 mM dimethyl adipate (0.0396 mmol) was irradiated in a J-Young NMR tube for 1 hour under AM1.5 solar irradiation. After 1 hour, an internal standard (1,1,2,2-tetrachloroethane) was added before the NMR spectrum of the reaction mixture was collected. The amount of product obtained was determined to be 0.0107 mmol. The rate, r_2, was determined to be 2.97×10^{-6} mmol s^{-1}. The absorbance of this sample was found to be 0.48 at 334 nm, and the fraction of light absorbed at 334 nm, f_2 was determined to be 0.67 ($f_2 = 1 - 10^{-0.48} = 0.67$). The previously obtained values for the n-butylammonium ferrioxalate actinometer in acetonitrile was $\Phi_1 = 0.966$ at 334 nm, $f_1 = 0.99$ at 334 nm, and $r_1 = 3.23 \times 10^{-5}$ mmol s^{-1} under the same AM1.5 solar irradiation.[43]

Hence, the quantum yield for the photoredox fluorination can be determined:

$$\Phi_2 = (f_1 \bullet \Phi_1 \bullet r_2) / (f_2 \bullet r_1)$$
$$= 0.99 \times 0.966 \times 2.97 \times 10^{-6} \text{ mmol } s^{-1} / 0.67 \times 3.23 \times 10^{-5} \text{ mmol } s^{-1}$$
$$= 0.13$$

DFT and TD-DFT calculations

All calculations in this work were performed using the Gaussian 09 D01 package.[47] The WB97XD DFT functional[68] was used in DFT and TD-DFT calculations together with the 6-311+G(2d) basis set. Preliminary calculations with other functionals suggested that they were not suitable for handling the open-shell systems involved in our study. Ultrafine grids were adopted for the numerical integration and default

convergence criteria and integration grids were utilized for the numerical integration in both DFT and TD-DFT calculations.

Conclusions

In summary, we employed nanosecond transient absorption spectroscopic studies to demonstrate the detailed elementary steps in a photoredox fluorination reaction that we reported previously. The time-resolved optical spectroscopy suggested a direct reaction only between the photoexcited AQN and Selectfluor® to form a transient AQN-Selectfluor® exciplex, which we have observed for the first time experimentally. No direct reaction was detected between AQN and the substrate. The transient AQN-Selectfluor® exciplex was substantiated by our TD-DFT calculations, which predicted an absorption spectrum that matched the difference spectra obtained experimentally. The AQN-Selectfluor® exciplex then reacted with sp^3 hybridized C-H bonds to form a secondary aliphatic and a Selectfluor® *N*-radical, both of which have thermally accessible activation barriers for exothermic F and H atom transfer processes, respectively. Although the radical chain reactions can propagate, the sub-unity quantum yield of 0.13 indicates that chain termination takes place during the catalytic process, thus requiring the AQN-Selectfluor® exciplex to sustain a controlled and chemoselective photodriven radical fluorination reaction at ambient temperatures.

Acknowledgements

H.S.S. is supported by MOE Tier 1 grants (M4011144, M4011611), the Nanyang Assistant Professorship (M4081154), and a NTU start-up grant (M4081012). We also thank the support from the Solar Fuels Laboratory at NTU and the Singapore-Berkeley Research Initiative for Sustainable Energy (SinBeRISE) CREATE Program. C.H.T. thanks NTU for the following grants: (M4080946.110 & M4081324.110) and an MOE Tier 1 (M4011372.110).

Notes and references

1. S. Purser, P. R. Moore, S. Swallow and V. Gouverneur, *Chem. Soc. Rev.*, 2008, **37**, 320-330.
2. J. Wang, M. Sánchez-Roselló, J. L. Aceña, C. del Pozo, A. E. Sorochinsky, S. Fustero, V. A. Soloshonok and H. Liu, *Chem. Rev.*, 2014, **114**, 2432-2506.
3. S. Swallow, in *Progress in Medicinal Chemistry*, eds. G. Lawton and D. R. Witty, Elsevier, 2015, vol. Volume 54, pp. 65-133.
4. P. W. Miller, N. J. Long, R. Vilar and A. D. Gee, *Angew. Chem. Int. Ed.*, 2008, **47**, 8998-9033.
5. M. Tredwell and V. Gouverneur, *Angew. Chem. Int. Ed.*, 2012, **51**, 11426-11437.
6. R. Berger, G. Resnati, P. Metrangolo, E. Weber and J. Hulliger, *Chem. Soc. Rev.*, 2011, **40**, 3496-3508.
7. T. Fujiwara and D. O'Hagan, *J. Fluorine Chem.*, 2014, **167**, 16-29.
8. P. A. Champagne, J. Desroches, J.-D. Hamel, M. Vandamme and J.-F. Paquin, *Chem. Rev.*, 2015, **115**, 9073-9174.
9. S. Protti, M. Fagnoni and D. Ravelli, *ChemCatChem*, 2015, **7**, 1516-1523.
10. W. Liu, X. Huang, M.-J. Cheng, R. J. Nielsen, W. A. Goddard and J. T. Groves, *Science*, 2012, **337**, 1322-1325.
11. S. Bloom, C. R. Pitts, D. C. Miller, N. Haselton, M. G. Holl, E. Urheim and T. Lectka, *Angew. Chem. Int. Ed.*, 2012, **51**, 10580-10583.
12. Y. Amaoka, M. Nagatomo and M. Inoue, *Org. Lett.*, 2013, **15**, 2160-2163.
13. J.-B. Xia, C. Zhu and C. Chen, *J. Am. Chem. Soc.*, 2013, **135**, 17494-17500.
14. X. Huang, W. Liu, H. Ren, R. Neelamegam, J. M. Hooker and J. T. Groves, *J. Am. Chem. Soc.*, 2014, **136**, 6842-6845.
15. C. R. Pitts, S. Bloom, R. Woltornist, D. J. Auvenshine, L. R. Ryzhkov, M. A. Siegler and T. Lectka, *J. Am. Chem. Soc.*, 2014, **136**, 9780-9791.
16. R. D. Chambers, M. Parsons, G. Sandford and R. Bowden, *Chem. Commun.*, 2000, 959-960.
17. R. D. Chambers, A. M. Kenwright, M. Parsons, G. Sandford and J. S. Moilliet, *J. Chem. Soc., Perkin Trans. 1*, 2002, 2190-2197.
18. S. Bloom, C. R. Pitts, R. Woltornist, A. Griswold, M. G. Holl and T. Lectka, *Org. Lett.*, 2013, **15**, 1722-1724.
19. C. R. Pitts, B. Ling, R. Woltornist, R. Liu and T. Lectka, *J. Org. Chem.*, 2014, **79**, 8895-8899.
20. X. Zhang, S. Guo and P. Tang, *Org. Chem. Front.*, 2015, **2**, 806-810.
21. K. K. Laali, A. Jamalian and C. Zhao, *Tetrahedron Lett.*, 2014, **55**, 6643-6646.
22. M. Rueda-Becerril, O. Mahé, M. Drouin, M. B. Majewski, J. G. West, M. O. Wolf, G. M. Sammis and J.-F. Paquin, *J. Am. Chem. Soc.*, 2014, **136**, 2637-2641.
23. S. Ventre, F. R. Petronijevic and D. W. C. MacMillan, *J. Am. Chem. Soc.*, 2015, **137**, 5654-5657.
24. X. Wu, C. Meng, X. Yuan, X. Jia, X. Qian and J. Ye, *Chem. Commun.*, 2015, **51**, 11864-11867.
25. J. C. T. Leung, C. Chatalova-Sazepin, J. G. West, M. Rueda-Becerril, J.-F. Paquin and G. M. Sammis, *Angew. Chem. Int. Ed.*, 2012, **51**, 10804-10807.
26. F. Yin, Z. Wang, Z. Li and C. Li, *J. Am. Chem. Soc.*, 2012, **134**, 10401-10404.
27. N. R. Patel and R. A. Flowers, *J. Org. Chem.*, 2015, **80**, 5834-5841.
28. S. Bloom, J. L. Knippel and T. Lectka, *Chem. Sci.*, 2014, **5**, 1175.
29. C. W. Kee, K. F. Chin, M. W. Wong and C.-H. Tan, *Chem. Commun.*, 2014, **50**, 8211-8214.
30. S. D. Halperin, H. Fan, S. Chang, R. E. Martin and R. Britton, *Angew. Chem. Int. Ed.*, 2014, **53**, 4690-4693.
31. J.-B. Xia, C. Zhu and C. Chen, *Chem. Commun.*, 2014, **50**, 11701-11704.
32. S. Bloom, M. McCann and T. Lectka, *Org. Lett.*, 2014, **16**, 6338-6341.
33. S. Ventre, F. R. Petronijevic and D. W. MacMillan, *J. Am. Chem. Soc.*, 2015, **137**, 5654-5657.
34. G. Moger and A. Rockenbauer, *React. Kinet. Catal. Lett.*, 1978, **8**, 125-129.
35. F. Minisci, *Synthesis*, 1973, **1973**, 1-24.
36. F. R. Mayo and C. Walling, *Chem. Rev.*, 1940, **27**, 351-412.
37. J. M. Tedder and J. C. Walton, *Acc. Chem. Res.*, 1976, **9**, 183-191.
38. C. Walling and F. R. Mayo, *Discuss. Faraday Soc.*, 1947, **2**, 295-303.

39. H. Gan and D. G. Whitten, *J. Am. Chem. Soc.*, 1993, **115**, 8031-8037.
40. J. R. Wolstenhulme, J. Rosenqvist, O. Lozano, J. Ilupeju, N. Wurz, K. M. Engle, G. W. Pidgeon, P. R. Moore, G. Sandford and V. Gouverneur, *Angew. Chem. Int. Ed.*, 2013, **52**, 9796-9800.
41. M. Rueda-Becerril, C. Chatalova Sazepin, J. C. Leung, T. Okbinoglu, P. Kennepohl, J.-F. o. Paquin and G. M. Sammis, *J. Am. Chem. Soc.*, 2012, **134**, 4026-4029.
42. A. Agiral, H. S. Soo and H. Frei, *Chem. Mater.*, 2013, **25**, 2264-2273.
43. S. Gazi, W. K. H. Ng, R. Ganguly, A. M. P. Moeljadi, H. Hirao and H. S. Soo, *Chem. Sci.*, 2015, **6**, 7130-7142.
44. J. W. Kee, Y. Y. Ng, S. A. Kulkarni, S. K. Muduli, K. Xu, R. Ganguly, Y. Lu, H. Hirao and H. S. Soo, *Inorg. Chem. Front.*, 2016, **3**, 651-662.
45. H. Shao, S. K. Muduli, P. D. Tran and H. S. Soo, *Chem. Commun.*, 2016, **52**, 2948-2951.
46. S. K. Muduli, S. Wang, S. Chen, C. F. Ng, C. H. A. Huan, T. C. Sum and H. S. Soo, *Beilstein J. Nanotechnol.*, 2014, **5**, 517-523.
47. M. J. Frisch, G. W. Trucks, H. B. Schlegel, G. E. Scuseria, M. A. Robb, J. R. Cheeseman, G. Scalmani, V. Barone, B. Mennucci, G. A. Petersson, H. Nakatsuji, M. Caricato, X. Li, H. P. Hratchian, A. F. Izmaylov, J. Bloino, G. Zheng, J. L. Sonnenberg, M. Hada, M. Ehara, K. Toyota, R. Fukuda, J. Hasegawa, M. Ishida, T. Nakajima, Y. Honda, O. Kitao, H. Nakai, T. Vreven, J. A. Montgomery Jr., J. E. Peralta, F. Ogliaro, M. J. Bearpark, J. Heyd, E. N. Brothers, K. N. Kudin, V. N. Staroverov, R. Kobayashi, J. Normand, K. Raghavachari, A. P. Rendell, J. C. Burant, S. S. Iyengar, J. Tomasi, M. Cossi, N. Rega, N. J. Millam, M. Klene, J. E. Knox, J. B. Cross, V. Bakken, C. Adamo, J. Jaramillo, R. Gomperts, R. E. Stratmann, O. Yazyev, A. J. Austin, R. Cammi, C. Pomelli, J. W. Ochterski, R. L. Martin, K. Morokuma, V. G. Zakrzewski, G. A. Voth, P. Salvador, J. J. Dannenberg, S. Dapprich, A. D. Daniels, Ö. Farkas, J. B. Foresman, J. V. Ortiz, J. Cioslowski and D. J. Fox, Revision D.01, Gaussian, Inc., Wallingford, CT, USA, 2009.
48. M. G. Holl, M. D. Struble, P. Singal, M. A. Siegler and T. Lectka, *Angew. Chem. Int. Ed.*, 2016, **55**, 8266-8269.
49. H. Görner, *Photochem. Photobiol.*, 2003, **77**, 171-179.
50. G. Zhu, J. Xu, G. Wu, H. Zhu, D. Long, S. Chen and S. Yao, *Int. J. Mol. Sci.*, 2006, **7**, 590-600.
51. T. Nakayama, K. Ushida, K. Hamanoue, M. Washio, S. Tagawa and Y. Tabata, *J. Chem. Soc., Faraday Trans.*, 1990, **86**, 95-103.
52. K. Tickle and F. Wilkinson, *Trans. Faraday Soc.*, 1965, **61**, 1981-1990.
53. B. E. Hulme, E. J. Land and G. O. Phillips, *J. Chem. Soc. Faraday Trans. 1*, 1972, **68**, 1992-2002.
54. S. A. Carlson and D. M. Hercules, *J. Am. Chem. Soc.*, 1971, **93**, 5611-5616.
55. B. S. Yamanashi and D. M. Hercules, *Appl. Spectrosc.*, 1971, **25**, 457-460.
56. K. Hamanoue, T. Nakayama, Y. Kajiwara, T. Yamaguchi and H. Teranishi, *J. Chem. Phys.*, 1987, **86**, 6654-6659.
57. T. Furuyu, C. A. Kuttruff and T. Ritter, *Curr. Opin. Drug Disc. Dev.*, 2008, **11**, 803-819.
58. A. G. Gilicinski, G. P. Pez, R. G. Syvret and G. S. Lal, *J. Fluorine Chem.*, 1992, **59**, 157-162.
59. M. A. Cismesia and T. P. Yoon, *Chem. Sci.*, 2015, **6**, 5426-5434.
60. M. D. Karkas, B. S. Matsuura and C. R. Stephenson, *Science*, 2015, **349**, 1285-1286.
61. K. K. Laali, A. Jamalian and C. Zhao, *Tetrahedron Lett.*, 2014, **55**, 6643-6646.
62. M. Ghosh, K. K. Singh, C. Panda, A. Weitz, M. P. Hendrich, T. J. Collins, B. B. Dhar and S. Sen Gupta, *J. Am. Chem. Soc.*, 2014, **136**, 9524-9527.
63. J. M. Kanabus-Kaminska, B. C. Gilbert and D. Griller, *J. Am. Chem. Soc.*, 1989, **111**, 3311-3314.
64. M. Hudlicky, *J. Fluorine Chem.*, 1985, **28**, 461-472.
65. A. Patel, Z. Chen, Z. Y. Yang, O. Gutierrez, H. W. Liu, K. N. Houk and D. A. Singleton, *J. Am. Chem. Soc.*, 2016, **138**, 3631-3634.
66. R. E. Plata and D. A. Singleton, *J. Am. Chem. Soc.*, 2015, **137**, 3811-3826.
67. C. G. Hatchard and C. A. Parker, *Proc. R. Soc. A*, 1956, **235**, 518-536.
68. Y. Zhao, N. E. Schultz and D. G. Truhlar, *J. Chem. Theory Comput.*, 2006, **2**, 364-382.